AFRL-RQ-WP-TP-2015-0149

CORRELATION OF HIFiRE-5 FLIGHT DATA WITH COMPUTED PRESSURE AND HEAT TRANSFER (POSTPRINT)

Joseph S. Jewell, James H. Miller, and Roger L. Kimmel

Vehicle Technology Branch and Hypersonic Sciences Branch
High Speed Systems Division

JUNE 2015

AIR FORCE RESEARCH LABORATORY
AEROSPACE SYSTEMS DIRECTORATE
WRIGHT-PATTERSON AIR FORCE BASE, OH 45433-7541
AIR FORCE MATERIEL COMMAND
UNITED STATES AIR FORCE

NOTICE AND SIGNATURE PAGE

Using Government drawings, specifications, or other data included in this document for any purpose other than Government procurement does not in any way obligate the U.S. Government. The fact that the Government formulated or supplied the drawings, specifications, or other data does not license the holder or any other person or corporation; or convey any rights or permission to manufacture, use, or sell any patented invention that may relate to them.

This report was cleared for public release by the USAF 88th Air Base Wing (88 ABW) Public Affairs Office (PAO) and is available to the general public, including foreign nationals.

Copies may be obtained from the Defense Technical Information Center (DTIC) (http://www.dtic.mil).

AFRL-RQ-WP-TP-2015-0149 HAS BEEN REVIEWED AND IS APPROVED FOR PUBLICATION IN ACCORDANCE WITH ASSIGNED DISTRIBUTION STATEMENT.

*//Signature//
ROGER L. KIMMEL
Project Manager
Hypersonic Sciences Branch
High Speed Systems Division

//Signature//
MICHAEL S. BROWN, Chief
Hypersonic Sciences Branch
High Speed Systems Division
Aerospace Systems Directorate

//Signature//
THOMAS A. JACKSON
Deputy for Science
High Speed Systems Division
Aerospace Systems Directorate

This report is published in the interest of scientific and technical information exchange, and its publication does not constitute the Government's approval or disapproval of its ideas or findings.

*Disseminated copies will show "//Signature//" stamped or typed above the signature blocks.

REPORT DOCUMENTATION PAGE

Form Approved
OMB No. 0704-0188

1. REPORT DATE *(DD-MM-YY)*	2. REPORT TYPE	3. DATES COVERED *(From - To)*
June 2015	Conference Paper Postprint	22 June 2014 – 22 June 2015

4. TITLE AND SUBTITLE
CORRELATION OF HIFiRE-5 FLIGHT DATA WITH COMPUTED PRESSURE AND HEAT TRANSFER (POSTPRINT)

5a. CONTRACT NUMBER
In-house

5b. GRANT NUMBER

5c. PROGRAM ELEMENT NUMBER
61102F

6. AUTHOR(S)
Joseph S. Jewell and Roger L. Kimmel (AFRL/RQHF)
James H. Miller (AFRL/RQHV)

5d. PROJECT NUMBER
3002

5e. TASK NUMBER
N/A

5f. WORK UNIT NUMBER
Q1FN

7. PERFORMING ORGANIZATION NAME(S) AND ADDRESS(ES)
Hypersonic Sciences Branch (AFRL/RQHF)
Vehicle Technology Branch (AFRL/RQHV)
High Speed Systems Division
Air Force Research Laboratory, Aerospace Systems Directorate
Wright-Patterson Air Force Base, OH 45433-7541
Air Force Materiel Command, United States Air Force

8. PERFORMING ORGANIZATION REPORT NUMBER
AFRL-RQ-WP-TP-2015-0149

9. SPONSORING/MONITORING AGENCY NAME(S) AND ADDRESS(ES)
Air Force Research Laboratory
Aerospace Systems Directorate
Wright-Patterson Air Force Base, OH 45433-7541
Air Force Materiel Command
United States Air Force

10. SPONSORING/MONITORING AGENCY ACRONYM(S)
AFRL/RQHF

11. SPONSORING/MONITORING AGENCY REPORT NUMBER(S)
AFRL-RQ-WP-TP-2015-0149

12. DISTRIBUTION/AVAILABILITY STATEMENT
Approved for public release; distribution unlimited.

13. SUPPLEMENTARY NOTES
PA Case Number: 88ABW-2015-2468; Clearance Date: 19 May 2015.

This paper was published in the proceedings of the 45th AIAA Thermophysics Conference, held June 22 - 26, 2015 in Dallas, TX.

14. ABSTRACT
The HIFiRE-5 test article was an elliptic cone with a 2.5-mm nose radius and 2:1 aspect ratio and a 7-degree minor-axis half-angle. The upper stage of the sounding rocket failed to ignite, resulting in a peak Mach number of about 3 instead of the target of 7. Flight heat flux and pressure data have been compared to α- and β-dependent CFD results for pressure distribution, as well as laminar and turbulent heat-transfer results. Computations were performed at three time points in the ascent trajectory. At each time point, five values each of angle of attack and yaw, ranging from -5.0° to 5.0°, were computed. CFD pressures, normalized with p_∞, were interpolated to the flight Mach numbers at specified times throughout the ascent and descent trajectories. At each flight time, α and β were estimated from measured pressure by determining the α-β combination that minimized the RMS difference between the measured and computed pressures. The vehicle attitude, as determined from measured pressure, was compared to the vehicle attitude derived from Inertial Measurement Unit (IMU) results for α and β from the flight. The two methods showed excellent agreement for the entirety of the ascent and reentry portions of the trajectory. A similar normalization of the laminar and turbulent heat transfer CFD results with St was compared to flight heat transfer measurements, and transition locations were inferred. Finally, a computational heat conduction analysis was made to verify assumptions inherent in the calculation of heat flux from temperature.

15. SUBJECT TERMS
boundary layer transition, hypersonic, ground test

16. SECURITY CLASSIFICATION OF:			17. LIMITATION OF ABSTRACT:	18. NUMBER OF PAGES	19a. NAME OF RESPONSIBLE PERSON (Monitor)
a. REPORT	b. ABSTRACT	c. THIS PAGE			Roger L. Kimmel
Unclassified	Unclassified	Unclassified	SAR	15	19b. TELEPHONE NUMBER *(Include Area Code)* N/A

AIAA Aviation
22-26 June 2015, Dallas, TX
45th AIAA Thermophysics Conference

Correlation of HIFiRE-5 Flight Data With Computed Pressure and Heat Transfer

Joseph S. Jewell,[1] James H. Miller,[2] and Roger L. Kimmel[3]

U.S. Air Force Research Laboratory, Wright-Patterson Air Force Base, OH 45433-7542

The HIFiRE-5 test article was an elliptic cone with a 2.5-mm nose radius and 2:1 aspect ratio and a 7-degree minor-axis half-angle. The vehicle was flown in April 2012. The upper stage of the sounding rocket failed to ignite, resulting in a peak Mach number of about 3 instead of the target of 7. Flight heat flux and pressure data (reduced from almost 300 thermocouples and 50 pressure transducers) have been compared to α- and β-dependent CFD results for pressure distribution, as well as laminar and turbulent heat-transfer results. Computations were performed at three time points in the ascent trajectory. At each time point, five values each of angle of attack and yaw, ranging from -5.0° to 5.0°, were computed. CFD pressures, normalized with p_∞, were interpolated to the flight Mach numbers at specified times throughout the ascent and descent trajectories. At each flight time, α and β were estimated from measured pressure by determining the α-β combination that minimized the RMS difference between the measured and computed pressures. The vehicle attitude, as determined from measured pressure, was compared to the vehicle attitude derived from Inertial Measurement Unit (IMU) results for α and β from the flight. The two methods showed excellent agreement for the entirety of the ascent and reentry portions of the trajectory. A similar normalization of the laminar and turbulent heat transfer CFD results with St was compared to flight heat transfer measurements, and transition locations were inferred. Finally, a computational heat conduction analysis was made to verify assumptions inherent in the calculation of heat flux from temperature.

Nomenclature

M	=	Mach number
Re	=	Reynolds number
p	=	pressure (Pa)
$\dot{q}$	=	heat flux (W/m^2)
St	=	Stanton number
T	=	temperature (K)
t	=	time (s)
u	=	velocity (m/s)
x	=	streamwise distance (m)
α	=	angle of attack (°)
β	=	yaw (°)
ϕ	=	angular location on vehicle surface (°)

Subscripts

e	boundary-layer edge conditions
tr	at transition
w	wall conditions
0	stagnation conditions
∞	freestream conditions

[1] Research Aerospace Engineer (NRC Research Associate), AFRL/RQHF. Member, AIAA.
[2] Lead Senior Aerospace Engineer, AFRL/RQHV. Associate Fellow, AIAA.
[3] Principal Aerospace Engineer, AFRL/RQHF. Associate Fellow, AIAA.

I. Introduction

The Hypersonic International Flight Research Experimentation (HIFiRE) program is a hypersonic flight test program executed by the Air Force Research Laboratory (AFRL) and the Australian Defence Science and Technology Organization (DSTO).[1, 2] Its purpose is to develop and validate technologies critical to next generation hypersonic aerospace systems. Candidate technology areas include, but are not limited to, propulsion, propulsion-airframe integration, aerodynamics and aerothermodynamics, high temperature materials and structures, thermal management strategies, guidance, navigation, and control, sensors, and system components such as munitions, submunitions and avionics. The HIFiRE program consists of extensive ground tests and computation focused on specific hypersonic flight technologies. Each technology program is designed to culminate in a flight test.

The philosophy of the HIFiRE program has been to identify and attack specific technology gaps in hypersonic flight. Preference is given to phenomena that are difficult to analyze computationally or with ground test. The intent of the program is to characterize the technology as fully as possible with a program of coordinated ground test and computation, culminating in a test flight for emphasis.

HIFiRE-5 is devoted to aerothermodynamic experiments, in particular transition on a three-dimensional geometry. References 3 and 4 contain a detailed description of the HIFiRE-5 configuration. The HIFiRE-5 vehicle is an elliptical cone with a 2:1 aspect ratio. It has a 7-degree half-angle on the minor axis and a 2.5-mm-radius nosetip. It is 0.86 m in length. The elliptic cone configuration was chosen as the test- article geometry based on extensive previous testing and analysis on elliptic cones (e.g. References 6-9). This prior work demonstrated that the 2:1 elliptic cone would generate significant crossflow instability at hypersonic flight conditions and potentially exhibit leading-edge transition. Preliminary inspection of the heat transfer data indicates that supersonic transition was observed during both the ascent and reentry portions of the trajectory.[10]

The HIFiRE-5 vehicle flew a ballistic trajectory, with no active attitude control. The elliptic cone test article remained attached to the second stage booster at all times, and relied on aerodynamic stability to minimize angle of attack. The payload spun at about 2 Hz to minimize trajectory dispersions. Since the payload was generally at some small angle of attack and spinning, any given point on the payload showed an oscillatory angle of attack and yaw (or equivalently, total angle of attack and roll) relative to the wind. Since the transition location is a function of vehicle attitude, it is important to determine accurately both the attitude and the time-dependent transition location.

Detailed calculations provide both an assessment of measured and computed quantities, and a means of reconstructing the flight. Previous analysis of the HIFiRE-5 flight one compared measured data to preliminary heating and pressure estimates.[4, 10] Since those results were published, detailed CFD calculations at actual flight conditions have become available. The first objective of the current work is to assess the accuracy of the computed pressures and heating rates. With confidence established in the computations, the computed pressures may then be used to back-calculate the vehicle attitude to establish a check of the attitude measured by the on-board IMU and GPS. Also, measured heating rates are subject to a number of uncertainties in terms of noise, boundary conditions, and lateral conduction effects. Plausible computed heating rates permit a quantification of these error sources. The final product of this effort will be a methodology for reconstructing flights of hypersonic vehicles, including the upcoming re-flight of HIFiRE-5.

II. Computational Methods

The flow solver used for the present CFD calculations is a modified version[11,12] of NASA's upwind parabolized Navier-Stokes (UPS) code[13]. Turbulence was modeled with the Baldwin-Lomax[14] turbulence model. To establish confidence that computational pressures could be used to determine the vehicle attitude independently of the on-board IMU and GPS, a grid refinement study was performed for three flight conditions. These conditions are listed in Table 1.

Table 1 Flight conditions used for grid refinement studies.

Time (s)	Mach	Re/m	Alpha (deg)	Beta (deg)	Velocity (m/s)	Density (kg/m^3)	Freestream Temp (K)	Wall Temp (K)
15.28289	2.01	3.0522×10^7	0.0694	0.0545	629.8897	0.760501	244.2351	293.15
18.48271	2.51	3.0232×10^7	-1.4527	-1.2191	761.0839	0.592388	229.454	308.15
23.59236	3.11	1.9753×10^7	0.7919	-2.0820	937.6307	0.311079	226.7277	333.15

These three times were all during the ascent phase of the flight and the measured heat transfer data indicates the flowfield is fully turbulent. The wall temperatures for each case were selected to best match the measured surface temperature on the vehicle which varies over the surface of the vehicle. Downstream of the nose, the surface temperature was largely uniform. The finest grid used in the present study consisted of 97 circumferential and 90 wall-normal nodes (97 × 90) per plane. Grid convergence for pressure and heat transfer for this grid has been confirmed through comparison with similar grids of 25 × 23 and 49 × 45 nodes. See Figure 1. The first cell height above the wall for the turbulent cases was 1.0×10^{-6} m. The average nondimensional wall distance, y^+, was less than one for all turbulent computations. The laminar grids utilized a cell height of 1.1×10^{-7} m ensuring that boundary layer details were captured. The turbulence model was started at 6 millimeters downstream of the nose. The number of steps in the x (axial) direction in each of three cases varied based on the velocity of the inflow, with more steps required to resolve higher u_∞ flows. The number of streamwise steps was 2884, 3486 and 5776 for Mach number conditions of 2.01, 2.51 and 3.11 respectively. The majority of cases utilized a linear increase in streamwise stepsize over 40-100 steps at the beginning of the computations and then maintained a constant stepsize thereafter. Default stability parameters were used for the UPS code, with EPSA, UWMACH set to 0.1 and 1.12 respectively for the majority of cases. The entropy smoothing parameter, EPSS, was set to 2×10^{-5} . Based on previous computational analyses, these parameters do not affect computational pressure results or heat transfer, but they can affect numerical stability.

Computations were performed at five values of α and β (-5.0°, -2.5°, -0.0°, 2.5° and 5.0°) for a total of 25 angle of attack/yaw combinations at each of the three conditions. The majority of cases were run for turbulent conditions, but some limited laminar computations were performed. Surface pressures did not show tangible differences between laminar and turbulent cases. Note that the definition of β for the UPS code results in a negative velocity component for a positive β therefore the circumferential angle, ϕ, was mirrored to be consistent with the flight data which utilizes a coordinate system where a positive β results in a positive velocity component.

Some of the computational results developed for the Mach 2.51 condition are presented in Figures 2-4. In Figure 2 the computed streamwise pressures are compared to measured flight pressures for the ϕ = 0 and ϕ = 90 rays. The agreement is good, with the computed pressures varying less than 5% from the measured flight pressures on the 90 degreee ray. It should be noted that the pressure-derived values for α and β are -0.85^o and -0.45^o respectively for this flight condition (see Section III). Although the pressure-derived values have not been used in computations at the time of writing, it is expected that the computational and experimental pressures presented in Figure 2 would show greater agreement if the CFD were performed with pressure-derived values for attitude, instead of the raw flight values shown in Table 1. (Indeed, this is a trivial conclusion as the corrected attitude is derived by minimizing the deviation between measured and computed pressures.)

In Figure 2, the computed circumferential pressures for laminar and turbulent results are compared to measured flight data. It is interesting to note that the measured flight pressures at 180 and 200 degrees have a difference of about 3% which could be taken as a representative uncertainty in the measured pressures. More details on the effects of grid refinement on pressures are presented in Ref. 11.

In Figure 3, the computed heat transfer rates are compared to measured flight data for laminar and turbulent conditions. The flow is turbulent within the locations of the instrumentation. Additionally in Figure 3, the effects of grid resolution are more apparent for turbulent flow than for laminar flow. The uncertainty for the flight data is about 15% for the ϕ = 0 location and 10% for the ϕ = 90 location. The change in grid density results in a percent change of similar magnitude for the coarse and fine grids for turbulent computations.

In Figure 4, the computed heat transfer rates are compared to measured flight data at two axial stations, x = 0.4m and x = 0.8m. The uncertainty in the flight data is of similar magnitude as in Figure 3. The percent change in turbulent heat transfer due to grid density is also similar. Note that for the present sideslip angle, the ϕ =270 location has higher pressures and heat transfer than the ϕ =90 location. However the area around the ϕ =90 location has more instrumentation than the ϕ =270 ray and so is better suited for detailed comparisons to the computational data. It should also be noted that multi-dimensional conduction effects, not accounted for in the flight data analysis led to flight heat transfer being overestimated near ϕ=0°, and underestimated near ϕ=90°. These effects are discussed in Section IV.

In addition to the three conditions during ascent, an additional flight condition was computed during the descent portion of the flight. This was done to enable comparisons between laminar and turbulent heat transfer results obtained during flight. These conditions correspond to a flight time of t = 193s: Mach = 2.64, $T\infty$ = 212.51 K, T_{wall} = 332.2 K, $\rho\infty$ = 0.1186 kg/m^3, α = -1.47^o and β = 0.1754^o . These conditions result in a freestream unit Reynolds number per meter of 6.54×10^6 . The grids used for the Mach 2.51 case were also used for the present case. Figure 5 includes results for the laminar and turbulent computations for the 0 and 90 degree rays. The agreement with laminar flight results is excellent, but the measured turbulent results appear to overshoot the computed turbulent

results. Section V discusses a possible explanation for this observed discrepancy. In Figure 6, the results for x = 0.4m and x = 0.8m show that the computed turbulent results are about 30% less than the measured flight data. It should be noted that, in order to obtain a transitional heating distribution, a flight condition with low Reynolds number and low heating had to be selected. The low heating led to larger scatter and uncertainty in the flight heating data at t = 193 seconds, compared to the ascent case of t = 18.48 seconds. In any case, it should be noted that the transition between laminar and turbulent flow is unambiguous, especially at x = 800 mm.

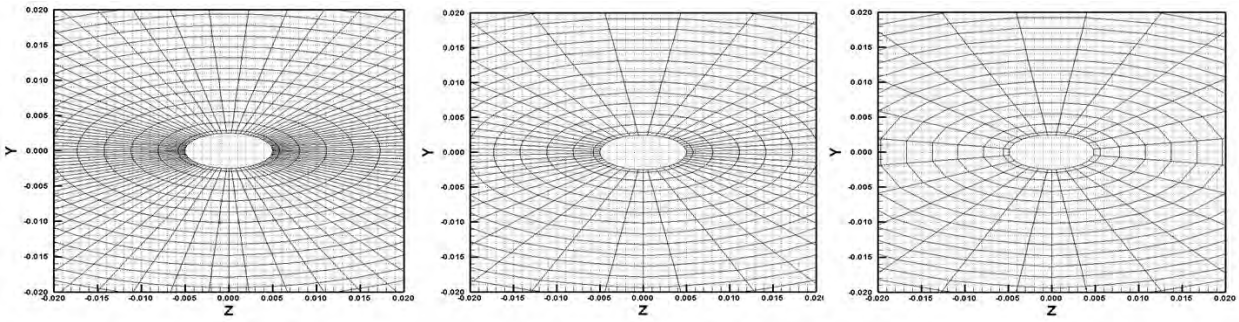

Figure 1 Surface grid structure for fine, medium and coarse grids.

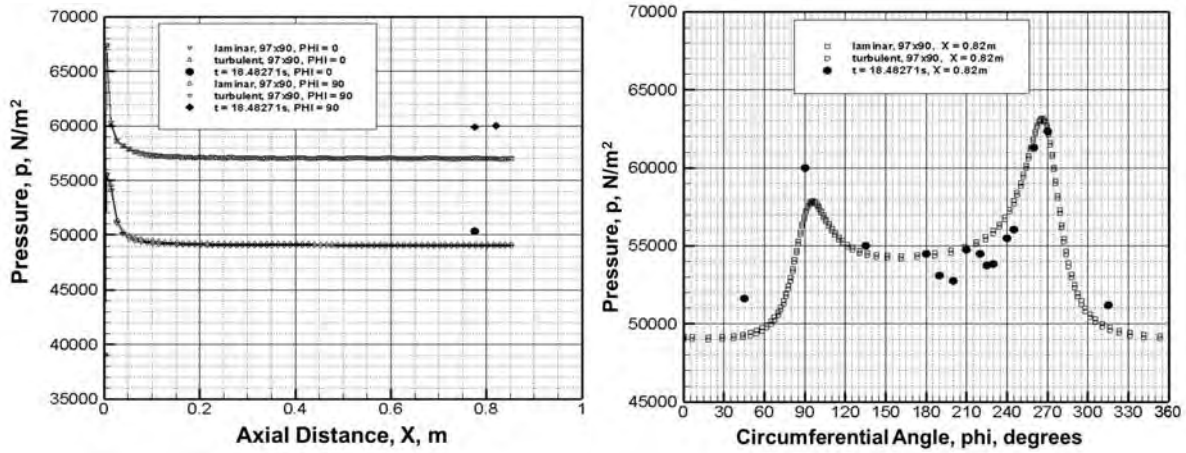

Figure 2 Computed and measured flight pressures for Mach 2.5 condition.

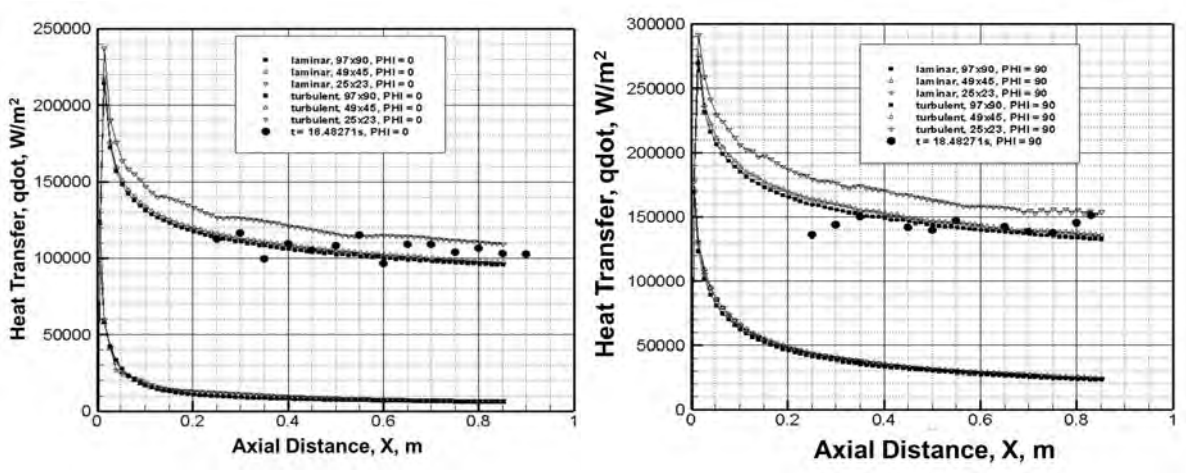

Figure 3 Heat transfer along centerline and ϕ = 90 ray for Mach 2.5 condition.

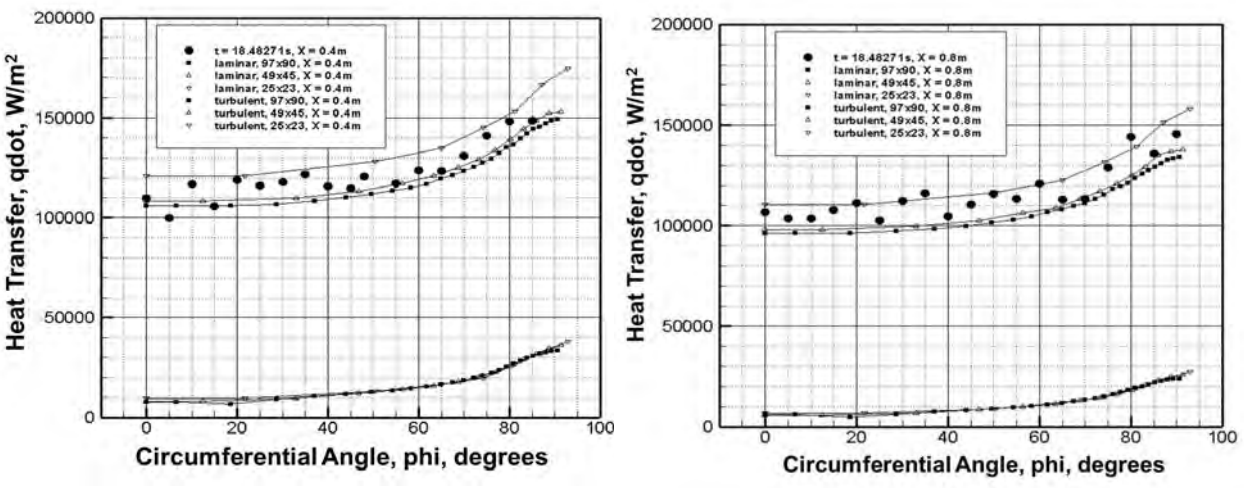

Figure 4 Heat transfer for X = 0.4m, 0.8m at Mach 2.5 condition.

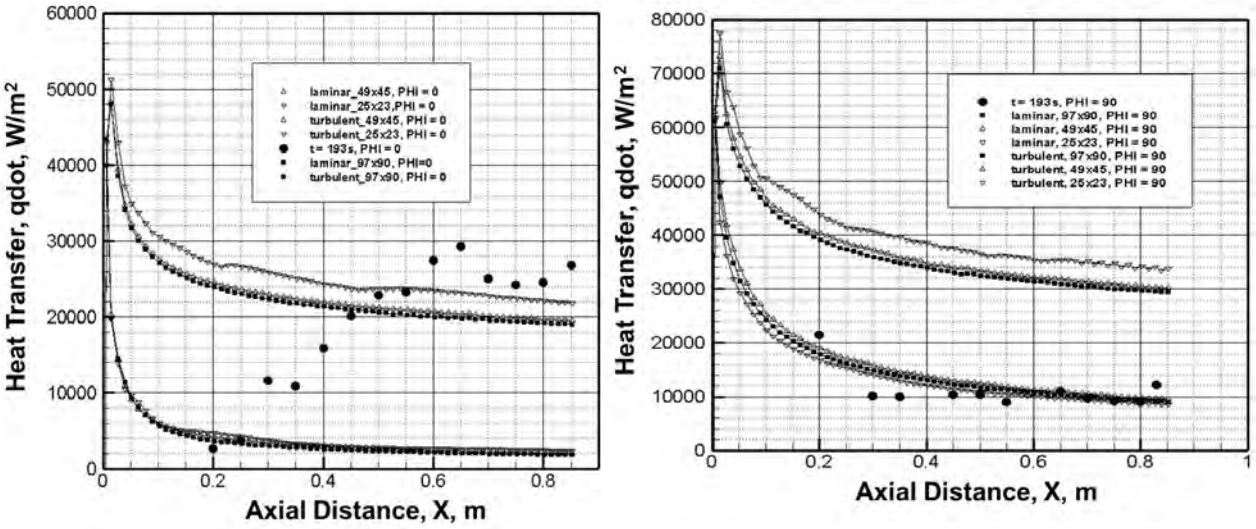

Figure 5 Heat transfer at Mach 2.6 condition along ϕ = 0 (centerline) and ϕ =90 rays.

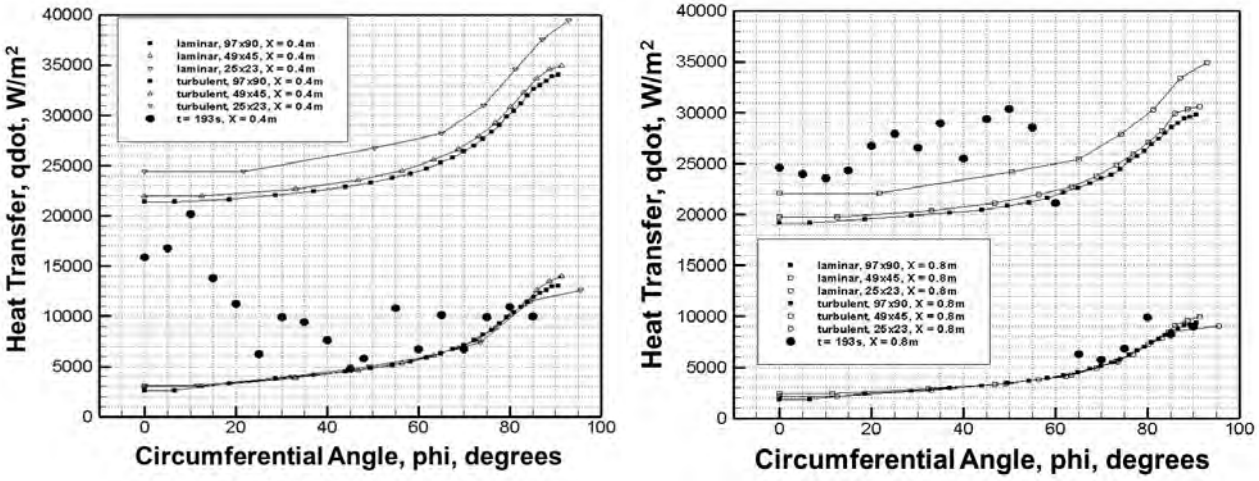

Figure 6 Heat transfer at Mach 2.6 conditions at X = 0.4m and 0.8m.

III. Pressure Distribution RMS Analysis and Comparison with CFD

Kulite pressure transducers measured local static pressures. Additionally, several pressure transducers were operated in differential mode to measure differential pressures 180 degrees apart on the vehicle to aid in attitude determination. Details of the HIFiRE-5 pressure transducers are found in Reference 10. Although directly computed CFD results are available at each freestream condition only at 25 discrete values of α and β, they may be smoothly interpolated to provide computational pressure information at intermediate values of α and β as well. A similar approach, utilizing a matrix of CFD solution points, has recently been used for the implementation of Flush Air Data Sensing (FADS) algorithms for reconstructing the Mars Science Laboratory entry, descent, and landing trajectory. [16] These interpolated CFD p values at the locations of 15 pressure transducers are calculated. The percentage root mean square differences between the set of transducers and the CFD results are presented in Figure 7 for the M =2.51 case. The RMS value is minimized at the value of α and β where the interpolated CFD results are most like the flight data, and this reconstructed angle of attack and yaw information is compared to the recorded IMU trajectory data from the same point in time. Good agreement is found for all three inflow conditions.

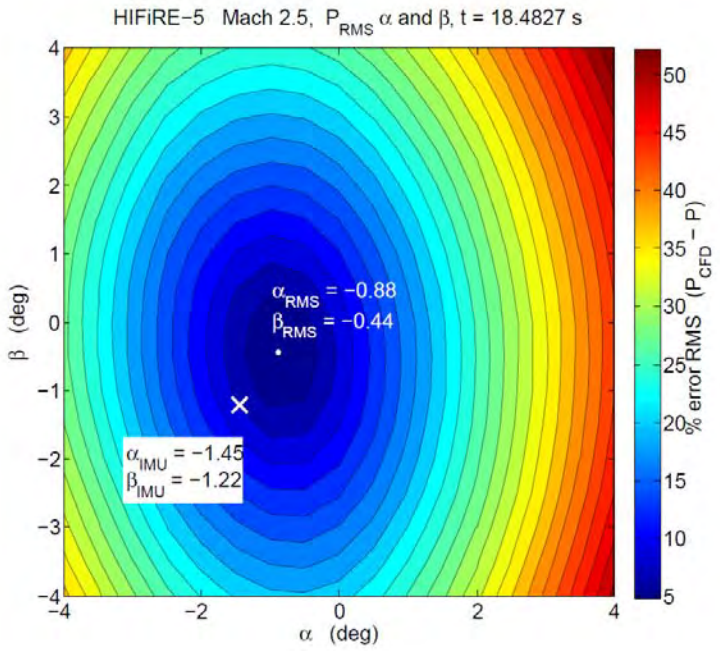

Figure 7 A contour plot in α and β of percent root mean square differences between the interpolated pressure CFD results at the locations of 15 pressure transducers distributed circumferentially around the HIFiRE-5 surface and the measured pressure from those transducers, at t = 18.4827s. The RMS value is minimized at the value of α and β where the interpolated CFD results are most like the flight data. This minimum is indicated with a white dot. The IMU value for the same time is indicated with a white ×.

It was infeasible to perform an array of 25 CFD cases for each time-step in the flight data set. However, normalizing each of the 25 cases for the three available pressure CFD conditions with p_∞ permits interpolations in Mach number to produce synthetic CFD results at time points other than the three discrete trajectory points for which CFD was actually performed. The RMS minimization procedure described above is then performed at each timepoint (at intervals of 0.01 s) for which there is sufficient pressure data over the entire ascent and reentry trajectory. These reconstructed results, when correlated with the Inertial Measurement Unit (IMU) results for α and β from the flight, show excellent agreement for the entirety of the ascent and reentry portions of the trajectory. Results from the ascent portion of the flight are presented in Figure 8. While the amplitude of α and β cyclic oscillations found in the reconstructed trajectory are larger in the IMU data for the first portion of the

ascent, good agreement with the mean values is observed, and excellent agreement with both the mean and oscillating α and β values for the latter portion of the ascent. Good agreement is also observed for the frequency of oscillation in both data sets.

This analysis of the vehicle attitude, inferred independently from pressure measurements, increases confidence in the attitude inferred from the IMU and GPS. This was the first HIFiRE flight using this GPS and IMU. The analysis indicates that, at least over these flight times and conditions, the GPS and IMU were able to measure vehicle attitude within 1 degree, with agreement generally better than that. The final version of this paper will include an estimate of the error associated with the payload attitude measurements, and additional analysis of attitude based on differential pressures.

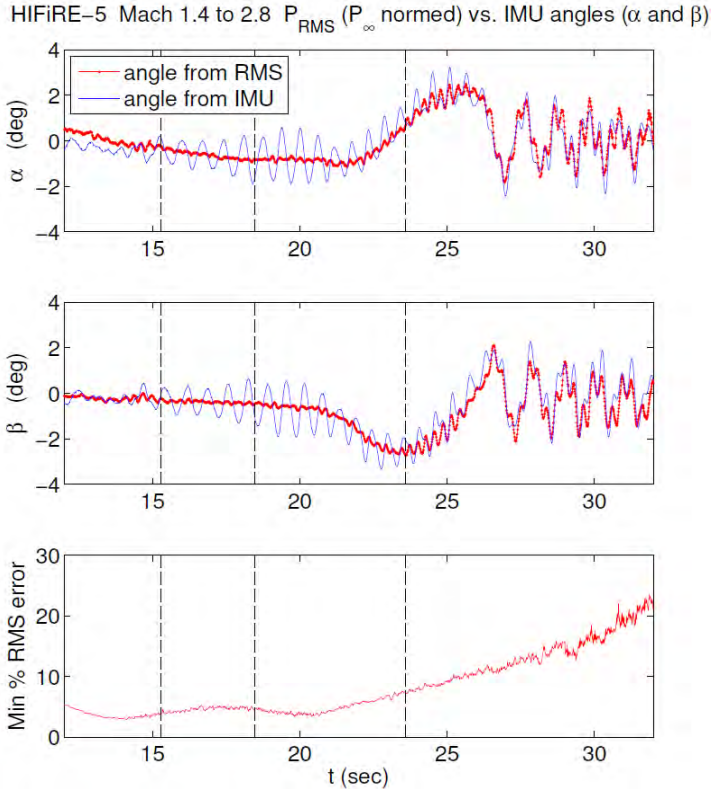

Figure 8 Angle of attack and yaw results for the ascent portion of the trajectory from the interpolation/RMS minimization routine compared with the IMU values. The trajectory times corresponding to the three computed CFD cases are indicated by the dashed black vertical lines on each plot.

IV. Heat Transfer Distribution Analysis and Comparison with CFD

The primary aerothermal instrumentation for HIFiRE-5 consisted of Medtherm Corporation coaxial thermocouples.[10] The values for heat flux $\dot{q}$ presented in this work were calculated, under an adiabatic assumption for the back-face temperature, from the front-face thermocouple temperatures by solving the transient 1-D heat equation. The FORTRAN QCALC subroutine was translated to Matlab for this purpose. QCALC assumes one-dimensional heat transfer and uses a second-order Euler explicit finite difference approximation to solve for the temperature distribution through the vehicle shell; heat flux is obtained from a second-order approximation to the derivative of the temperature profile at the outer surface.[15]

Laminar and turbulent heat transfer calculations at the three time points described in Section II were normalized by Stanton number based on the wall and stagnation temperatures:

$$\mathrm{St} = \frac{\dot{q}}{(T_0 - T_w)\rho u_\infty c_p}$$

Stagnation temperature is used in the data reduction, since it is easier to define than recovery temperature, and wall temperatures were well away from recovery temperatures. As described in Section III for the pressure results

normalized by p_∞, this St normalization permits α- and β-dependent interpolations in Mach number to produce synthetic laminar and turbulent heat transfer CFD results at time points other than the three discrete trajectory points for which CFD was actually performed. This analysis is performed (at intervals of 0.01s) at every time point for which there is sufficient heat transfer data over the entire ascent and reentry trajectory. Results for the location of one thermocouple (x=0.8m, ϕ=90°), from which the time of laminar-turbulent transition at this location may be inferred, are presented in Figure 9.

The results in Figure 9 indicate good agreement between the measured and computed heat transfer. The difference between laminar and turbulent heating is sufficiently large that boundary layer transition is readily identifiable. Continued analysis, to be presented in the final version of this paper, will include assessment of the measured and computed heating uncertainties, and a reassessment of transition times and Reynolds numbers, as based on computed heating rates.

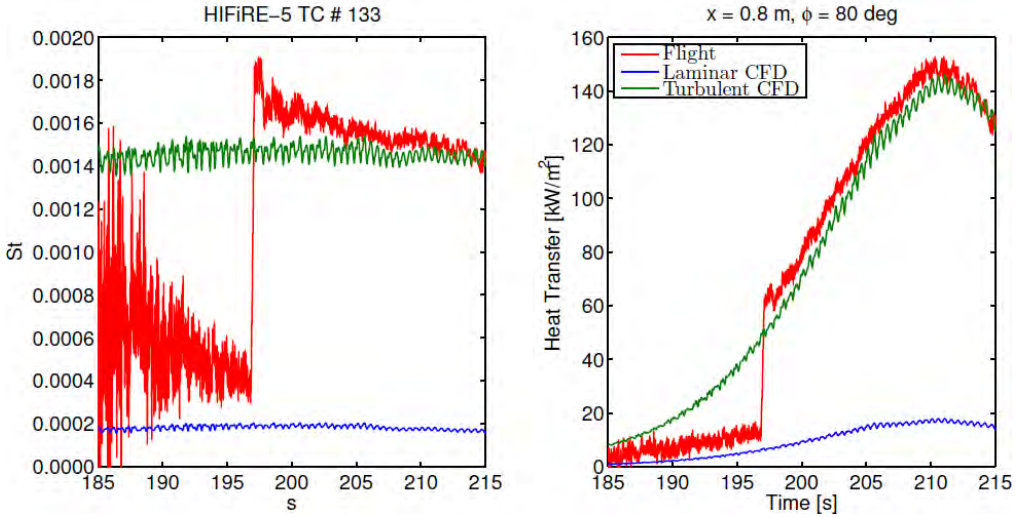

Figure 9 Computed laminar and turbulent heat transfer results for the reentry portion of the trajectory combined with flight data, both taken at the location of one thermocouple. Left: data normalized by Stanton number (note that small values for heat transfer at the beginning of reentry result in large variation, for a given experimental uncertainty, in St terms). Right: physical variables. Laminar to turbulent transition is clearly observed in this location at t = 197 s. The oscillations in the interpolated CFD curves are the result of changing angle of attack and yaw.

V. Axisymmetric Shell Heat Conduction Computations

Although measured heat transfer generally agreed well with computed heat transfer, some discrepancies existed, especially at lower heating levels. Since the heat transfer data reduction used a one-dimensional conduction assumption, it was possible that some discrepancies arose from multi-dimensional conduction effects. In order to investigate this, the TOPAZ unsteady conduction code was used to assess multi-dimensional heating. TOPAZ had been used previously to examine lateral conduction effects, but realistic heating distributions were not available when this prior effort was accomplished.[10]

The methodology for this analysis was to calculate time-dependent heating temperatures in the aeroshell, including convective heating and conduction, and then analyze these temperatures as if they were experimental thermocouple data. In this way, the input convective heating would be exactly known, and the heating rates inferred from the computed shell temperatures would be subject to realistic conduction effects. The computed PNS convective heat transfer rates served as convective boundary conditions to TOPAZ. TOPAZ calculations then provided the outer and inner surface aeroshell temperatures. These computed temperatures then served as inputs to the same QCALC inverse solver that was used to derive heat transfer from the flight thermocouple data. This analysis thus provided a semi-quantitative assessment of lateral conduction errors in the flight data analysis.

This analysis was semiquantitative for two reasons. First, the actual flight heating was unknown. The computed convective heating however, was at least a plausible approximation of flight heating. Secondly, only a 2D/axisymmetric version of TOPAZ was available, and turbulent-laminar transition was only approximately modeled. Nevertheless, separate calculations could approximate axial and circumferential conduction effects. These approximations were not objectionable, since the objective of the study was not to recreate or calibrate the data reduction, but to provide some bounds on lateral conduction errors.

In the current study, the aeroshell was modeled first as an elliptic cylinder to model circumferential conduction. The grid for this analysis was a 90° arc of an elliptic cylinder with the same dimensions as HIFiRE-5 at x=400mm. Computed heat transfer rates were applied as convective boundary conditions on the outer surface of the shell. Transition was modeled as a simple step change from turbulent to laminar heating at the appropriate time at each angular location. The flight data in some cases displayed multiple excursions between fully laminar and fully turbulent heating over a period of time during transition. Given the approximate nature of the analysis, this was not deemed to be a significant source of error. In the second step of the analysis, a streamwise section of a 7-degree circular cone was used to model axial conduction. Streamwise centerline and leading edge heating distributions were imposed as boundary conditions in two separate calculations. The backface boundary condition was adiabatic in all cases.

Figure 10 shows isotherms for the elliptic cylinder at x=400mm for t=20 seconds, near the time of maximum ascent heating, and t=32 seconds, when convective heating had dropped sharply. At t=20 seconds, the dominant temperature gradient is normal to the surface, indicating that the assumption of 1D conduction into the aeroshell was largely valid. By t=32 seconds, the dominant temperature gradient is in the circumferential direction, indicating that lateral conduction at this time likely dominated over convective heating and conduction into the shell.

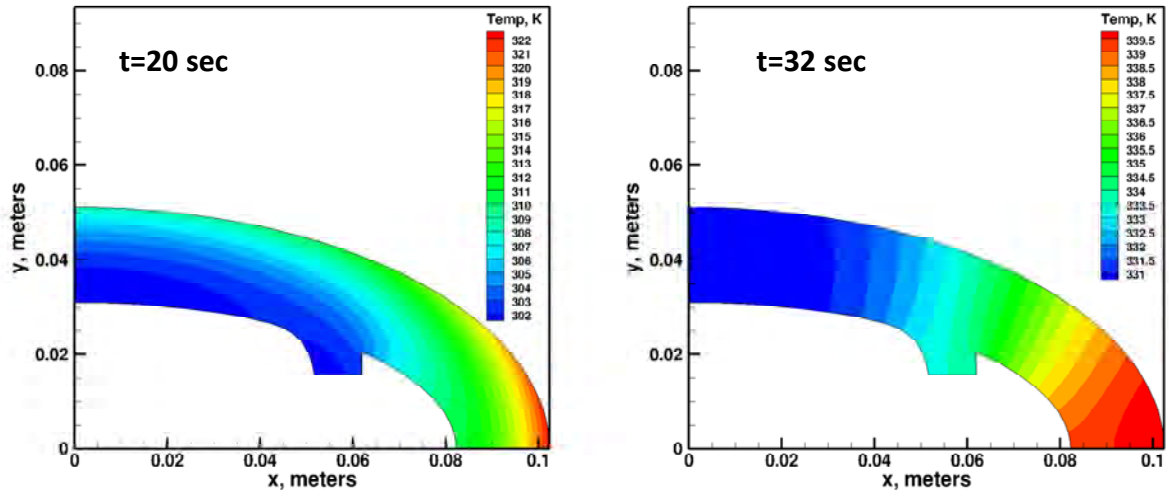

Figure 10 Measured and computed temperature history near the HIFiRE-5 leading edge at x=400 mm.

Figure 11 compares the input and derived heating histories for the elliptic cylinder at the centerline (ϕ=0°) and leading edge (ϕ=90°). The green lines indicate the heating rates that were input to TOPAZ as convective boundary conditions. The red lines indicate the heating rates that were inferred using the QCALC inverse solver, with the TOPAZ-calculated temperature histories as input. The effect of circumferential conduction is apparent at both locations. The derived heating follows the input heating rather closely until near maximum heating. After this time, the inverse solver overestimates the centerline heating rates by a fairly constant amount of about 12 kW/m^2. This overestimation is due to the conduction of heat from warmer parts of the shell into this location. At the leading edge, the inverse solver underestimates the convective heat flux into the surface, since heat is being conducted away from the leading edge. After the boundary layer transitions, the derived heat flux at the leading edge is actually negative, because conduction away from this region is greater than convective heating into the surface.

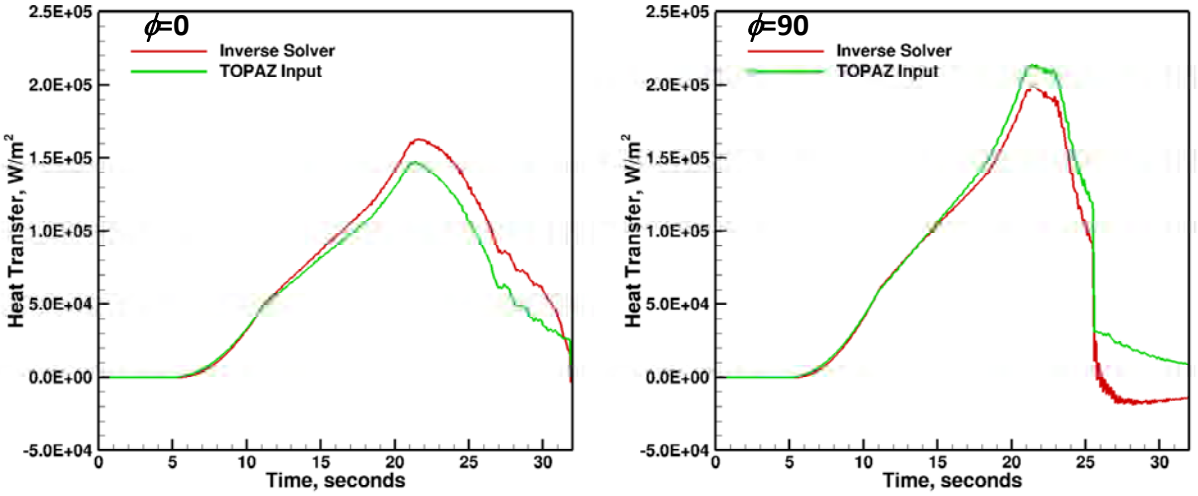

Figure 11 Input and derived heating rates for the elliptic cylinder.

Figure 12 illustrates the effects of axial conduction for a 7° half-angle circular cone. The green lines indicate the TOPAZ convective boundary conditions, and red lines indicate heating rates derived from the inverse solver. Again, the input and derived heating rates are comparable until the maximum heating times. After this time, the inverse solver overestimates heating at all circumferential locations, since heat is being conducted from the nose aft. The axial conduction error at this location is smaller than the circumferential conduction error. The axial conduction to some extent offsets circumferential conduction near the leading edge. On the centerline, however, errors due to axial and circumferential conduction are additive.

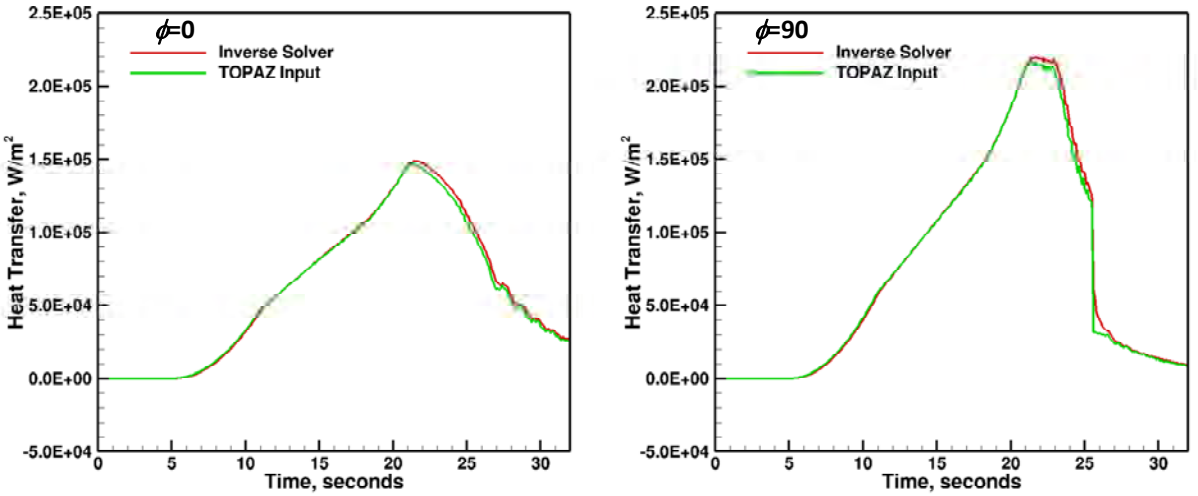

Figure 12 Input and derived heating rates for the circular cone at *x*=400 mm.

Of the three vehicle stations where thermocouples were arrayed around the circumference, the *x*=400 mm station would have possessed the maximum axial and circumferential conduction errors, since the temperature gradients were at a maximum. This analysis indicates that near the centerline, flight heating rates were overestimated at *t*=25 seconds by approximately 27 kW/m^2. On the leading edge at this time, flight heating rates would have been underestimated by about 16 kW/m^2. During reentry, lateral conduction errors would have been less since the payload temperature had largely equilibrated prior to reentry, minimizing temperature gradients in both directions. This analysis is only approximate in nature, but it indicates the feasibility of more

sophisticated thermal analysis of configurations like HIFiRE-5, either using a 3D inverse solver, or multiple iterations with a 3D unsteady conduction solver.

VI. Conclusions

It has been demonstrated that normalized pressure CFD results may be used to infer angle of attack and yaw from a set of pressure transducers distributed over the body of the HIFiRE-5 flight test article. Interpolations in Mach number have been correlated with the Inertial Measurement Unit results for α and β from the flight, with excellent agreement for the entirety of the ascent and reentry portions of the trajectory. A similar normalization of the laminar and turbulent heat transfer CFD results with St has been compared to flight heat transfer measurements, and transition locations have been inferred. Computational heat conduction analysis has demonstrated that the assumptions inherent in the calculation of heat flux from temperature are reasonable for much of the HIFiRE-5 trajectory, and may account for discrepancies between measured and computed laminar and turbulent heat transfer levels. If so, further work to characterize lateral and axial conduction would enable a correction factor to be applied to the thermocouple-derived measurement of $\dot{q}$ for the portions of the trajectory where this effect is significant.

The analysis presented in this paper indicates that is feasible to reconstruct the HIFiRE-5 flight using a synthesis of measured and computed data. It may be possible to extend this type of analysis to future flights of HIFiRE and other hypersonic vehicles.

Acknowledgments

HIFiRE flight 5 was supported by the United States Air Force Research Laboratory and the Australian Defence Science and Technology Organisation and was carried out under Project Agreement AF-06-0046. J. S. Jewell is supported by the National Research Council Research Associateship. The authors thank Dr. Thomas J. Juliano for his helpful advice on HIFiRE-5 data reduction. Many thanks are extended to the Andøya Rocket Range of Norway and DLR/Moraba, and all members of the DSTO AVD Team Brisbane. The HIFIRE-5 first-stage rocket motor was procured from CTA Instituto de Aeronáutica e Espaço (IAE, Brazil) by the DLR. The authors gratefully acknowledge the efforts and support of Douglas Dolvin, AFRL/RQHV and John Schmisseur and Rengasamy Ponnappan of the Air Force Office of Scientific Research.

References

[1]Douglas J. Dolvin. Hypersonic International Flight Research and Experimentation (HIFiRE): Fundamental sciences and technology development strategy. AIAA Paper 2008-2581, April 2008.

[2]Douglas J. Dolvin. Hypersonic International Flight Research and Experimentation technology development and flight certification strategy. AIAA Paper 2009-7228, October 2009.

[3]R. L. Kimmel, D. Adamczak, K. Berger, and M. Choudhari. HIFiRE-5 flight vehicle design. AIAA Paper 2010-4985, June 2010.

[4]R. L. Kimmel, D. Adamczak, T. J. Juliano, and the DSTO AVD Brisbane Team. HIFiRE-5 flight test preliminary results. AIAA Paper 2013-0377, January 2013.

[5]R. L. Kimmel and J. Poggie. Three-dimensional hypersonic boundary layer stability and transition. Technical Report WL-TR-97-3111, Air Force Research Laboratory, Wright-Patterson Air Force Base, OH 45433-7542, December 1997.

[6]R. L. Kimmel, J. Poggie, and S. N. Schwoerke. Laminar-turbulent transition in a Mach 8 elliptic cone flow. AIAA Journal, 37(9):1080–1087, September 1999.

[7]Michael S. Holden. Experimental studies of laminar, transitional, and turbulent hypersonic flows over elliptic cones at angle of attack. Technical Report AFRL-SR-BL-TR-98-0142, Air Force Office of Scientific Research, Bolling Air Force Base, DC, 1998.

[8]J. D. Schmisseur, S. P. Schneider, and S. H. Collicott. Response of the Mach-4 boundary-layer on an elliptic cone to laser-generated freestream perturbations. AIAA Paper 1999-0410, January 1999.

[9]I. J. Lyttle and H. L. Reed. Use of transition correlations for three-dimensional boundary layers within hypersonic flows. AIAA Paper 1995-2293, June 1995.

[10]T. J. Juliano, D. Adamczak, and R. L. Kimmel. HIFiRE-5 Flight Test Heating Analysis. AIAA paper 2014-0076, January 2014.

[11]J.H. Miller, D.W. Adamczak, and J.A. Tancred. Flight Data Reduction for HIFiRE Flight 5. 38DCASS-129 presentation, Dayton-Cincinnati Aerospace Sciences Symposium, Dayton, OH, March 2013.

[12]J.C. Tannehill, J.H. Miller, and S.L. Lawrence. Development of an Iterative PNS Code for Separated Flows. AIAA Paper 99-3361, June 1999.

[13]S.L. Lawrence, D.S. Chaussee, and J.C. Tannehill. Application of an Upwind Algorithm to the Three-Dimensional Parabolized Navier-Stokes Equations. AIAA Journal, Vol. 28, No. 6, 1990, pp. 971,972.

[14]B.S. Baldwin and H. Lomax. Thin Layer Approximation and Algebraic Model for Separated Turbulent Flows, AIAA Paper 78-257, Jan. 1978.
[15]C. F. Boyd and A. Howell. Numerical investigation of one-dimensional heat-flux calculations. Technical Report NSWCDD/TR-94/114, Dahlgren Division Naval Surface Warfare Center, Silver Spring, MD 20903-5640, October 1994.
[16]C. D. Karlgaard, P. Kutty, M. Schoenberge, M. M. Munk, A. Little and C. A. Kuhl. Mars Science Laboratory Entry Atmospheric Data System Trajectory and Atmosphere Reconstruction. Journal of Spacecraft and Rockets, Vol. 51, No. 4, 2014, pp. 1029-1047.